© JUL 2026 | IRE Journals | Volume 10 Issue 1 | ISSN: 2456-8880
DOI: https://doi.org/10.64388/IREV10I1-1719722

Chemical Reaction of Prandtl-Eyring Hydromagnetic Nanofluid Flow in Porous Media: Thermophoretic and Brownian Motion Effects

J.O. AJILORE[1], S.O. SALAWU[2], O.K. ONANUGA[3], A.A. ABDURASID[4], I. A. IDOWU[5]
[1,4,5]Department of Mathematical Sciences, Lagos State University of Science and Technology, Ikorodu, Nigeria
[2]Department of Mathematics, Federal University of Technology and Environmental Sciences, Iyin-Ekiti, Nigeria
[3]Department of Physical Sciences, Lagos State University of Science and Technology, Ikorodu, Nigeria.

***Abstract-** This study investigates the steady two-dimensional magnetohydrodynamic (MHD) flow of an electrically conducting Prandtl-Eyring nanofluid over a stretching sheet embedded in a porous medium, incorporating the effects of Brownian motion, thermophoresis, and a first-order chemical reaction. The Buongior nonanofluid model is employed to describe nanoparticle transport mechanisms, while similarity transformations reduce the governing nonlinear partial differential equations to a coupled system of nonlinear ordinary differential equations. The resulting boundary-value problem is solved numerically using a shooting technique combined with the classical fourth-order Runge-Kutta method, and the accuracy of the numerical procedure is verified through comparison with existing results available in the literature. The influence of key physical parameters, including the magnetic, porous medium, Prandtl-Eyring fluid, Brownian motion, thermophoresis, Prandtl, Lewis, and chemical reaction parameters, on the velocity, temperature, and concentration fields is systematically examined. The results reveal that increasing magnetic field strength and porous resistance suppress the fluid velocity while enhancing the wall shear stress. Brownian motion and thermophoresis significantly increase the thermal boundary layer thickness, whereas higher Prandtl and Lewis numbers reduce the temperature and concentration distributions, respectively. Furthermore, stronger chemical reactions reduce nanoparticle concentration, while the surface heat transfer rate increases with the Prandtl number but decreases with increasing Brownian motion and thermophoresis. These findings provide valuable insight into the transport characteristics of non-Newtonian nanofluids in porous media and may contribute to the design of advanced thermal management systems, energy devices, and chemically reactive industrial processes.*

***Keywords:** Brownian Motion, Chemical Reaction, Porous Medium, Prandtl-Eyringnano Fluid, Thermophoresis.*

I. INTRODUCTION

Nanofluids have attracted considerable attention over the past three decades because of their superior thermal transport characteristics compared with conventional heat transfer fluids. By dispersing nanoparticles in base fluids, nanofluids exhibit enhanced thermal conductivity, improved heat-transfer efficiency, and improved energy-transport performance, making them suitable for applications in electronic cooling, solar energy systems, biomedical engineering, nuclear reactors, and advanced manufacturing processes [1-3]. Since the pioneering work of Choi [1], extensive theoretical, numerical, and experimental studies have been devoted to understanding the transport mechanisms governing nanofluid flow under different physical conditions.

Among the various mathematical models proposed for nanofluids, the Buongiorno model [4] remains one of the most widely accepted because it accounts for the relative motion between nanoparticles and the base fluid. The model identifies Brownian and thermophoretic diffusion as the dominant slip mechanisms governing nanoparticle transport, thereby providing a more realistic representation of coupled heat and mass transfer than homogeneous nanofluid models. Consequently, numerous investigations have employed the Buongiorno model to study boundary-layer transport over stretching and shrinking surfaces.Boundary-layer flow over stretching sheets has significant practical importance in polymer extrusion, wire drawing, glass-fibre production, continuous casting, and metallurgical processing. In these applications, accurate prediction of velocity, temperature, and concentration distributions is essential for controlling product quality and improving thermal efficiency [5-9]. The incorporation of a transverse magnetic field introduces MHD effects that are particularly relevant in electrically conducting fluids. The induced Lorentz force modifies the momentum transport, suppresses fluid motion, and alters thermal characteristics, making MHD nanofluid models indispensable in electromagnetic cooling, crystal growth, plasma engineering, and metallurgical technologies [10-12].

Although Newtonian fluids have been extensively studied, many industrial fluids exhibit non-Newtonian rheological characteristics that cannot be adequately represented by Newtonian constitutive laws [13-15]. The Prandtl-Eyring fluid model has emerged as an important non-Newtonian model because it successfully captures shear-thinning behaviour without the singularities associated with many empirical rheological models. Owing to its mathematical simplicity and physical relevance, the Prandtl-Eyring model has been successfully applied to the analysis of polymer solutions, lubricants, biological fluids, paints, and other complex materials (Malik et al. [16]). Several researchers have examined MHD Prandtl-Eyring fluid flow over stretching surfaces while incorporating additional transport phenomena such as thermal radiation, viscous dissipation, heat generation, and convective boundary conditions Hayat et al. [17].

Another important aspect influencing fluid transport is the presence of porous media. Fluid flow through porous structures occurs naturally in geothermal reservoirs, filtration systems, catalytic reactors, packed-bed heat exchangers, petroleum recovery, groundwater hydrology, and biological tissues [18,19]. The porous matrix introduces additional resistance to fluid motion, modifies the momentum boundary layer, and significantly influences both heat and mass transport. Likewise, chemical reactions play a crucial role in many engineering and environmental systems, including catalytic combustion, chemical processing, pollutant transport, fuel cells, biochemical reactors, and pharmaceutical manufacturing [20.21]. In particular, first-order homogeneous chemical reactions substantially affect species concentrations and mass-transfer rates, thereby influencing the overall transport process.

Recent studies have investigated various combinations of MHD effects, non-Newtonian fluids, porous media, Brownian motion, thermophoresis, and chemical reactions. However, most of these investigations rely exclusively on numerical simulations and often neglect the simultaneous interactions among Prandtl-Eyring rheology, porous-medium resistance, nanoparticle transport mechanisms, and chemically reactive species within a unified mathematical framework [23-25]. Furthermore, relatively few studies have provided comprehensive validation of numerical solutions together with detailed analyses of the combined influence of these parameters on engineering quantities such as wall shear stress, heat transfer rate, and mass transfer rate.

Motivated by these observations, the present study investigates the steady two-dimensional MHD flow of a Prandtl-Eyringnanofluid over a stretching sheet embedded in a porous medium, incorporating Brownian motion, thermophoresis, and a first-order chemical reaction, based on the Buongiornonanofluid model. Similarity transformations are employed to convert the governing nonlinear partial differential equations into a coupled system of nonlinear ordinary differential equations, which are solved numerically using the shooting method combined with the classical fourth-order Runge-Kutta algorithm. The numerical procedure is validated through comparison with previously published results. The effects of the magnetic parameter, porous medium parameter, Prandtl-Eyring fluid parameter, Brownian motion parameter, thermophoresis parameter, Prandtl number, Lewis number, and chemical reaction parameter on the velocity, temperature, and concentration fields, together with the wall shear stress, surface heat transfer rate, and mass transfer rate, are systematically examined. The findings provide useful insight into the thermal and transport

© JUL 2026 | IRE Journals | Volume 10 Issue 1 | ISSN: 2456-8880
DOI: https://doi.org/10.64388/IREV10I1-1719722

behaviour of non-Newtonian nanofluids and offer guidance for the design and optimization of advanced thermal systems involving porous media and chemically reactive flows.

Research Gap and Objectives

Despite the substantial body of research on magnetohydrodynamic (MHD) nanofluid flows over stretching surfaces, several important challenges remain unresolved. Existing studies have predominantly focused on either Newtonian nanofluids or isolated non-Newtonian fluid models while considering only a limited number of transport mechanisms. In particular, relatively few investigations have examined the combined effects of Prandtl-Eyring non-Newtonian rheology, porous-medium resistance, Brownian motion, thermophoretic diffusion, and homogeneous first-order chemical reactions within the framework of the Buongior nonanofluid model. Furthermore, most available studies focus on local flow characteristics without providing a comprehensive analysis of how these physical mechanisms interact to influence engineering performance indicators such as wall shear stress, heat transfer rate, and mass transfer rate. Although numerical approaches are widely employed, comparative validation of the computational methodology against benchmark solutions remains limited, reducing confidence in the predictive capability of many existing models.

II. MATHEMATICAL FORMULATION

A steady, two-dimensional Prandtl-Eyringnanofluid flow is considered over a stretchable sheet aligned along the x-axis, where the sheet stretches linearly with velocityU(x) =ax. A uniform magnetic field of strength B_0 is applied perpendicular to the surface (in the y-direction) to control the flow behaviour. The fluid flows through a porous medium and experiences both Brownian motion and thermophoresis effects. A first-order chemical reaction is also incorporated into the concentration equation. Figure 1 illustrates the physical configuration and coordinate system.

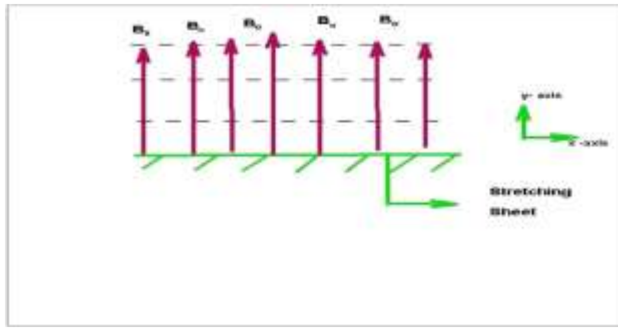

Figure 1: Flow geometry of the problem

Continuity equation:

$$\frac{\partial u}{\partial x} + \frac{\partial v}{\partial y} = 0 \qquad (1)$$

Momentum equation:

$$u\,\frac{\partial u}{\partial x} + v\,\frac{\partial u}{\partial y} = \frac{A}{\rho_C}\frac{\partial^2 u}{\partial y^2} - \frac{A}{2\rho C^3}\left(\frac{\partial u}{\partial y}\right)^2 \frac{\partial^2 u}{\partial y^2} - \frac{\sigma B_0^2}{\rho}\,u - \frac{\nu}{k_1}\,u = 0$$

(2)

Energy Equation:

$$u\left(\frac{\partial T}{\partial x}\right) + v\left(\frac{\partial T}{\partial y}\right) = \alpha_1\left(\frac{\partial^2 T}{\partial y^2}\right) + \tau\,\left(D_B\left(\frac{\partial c}{\partial y}\right)\left(\frac{\partial T}{\partial y}\right) + \frac{D_T}{T_\infty}\left(\frac{\partial T}{\partial y}\right)^2\right)$$

(3)

Concentration equation:

$$\left(\frac{\partial c}{\partial x}\right)u + \left(\frac{\partial c}{\partial y}\right)v = D_B\,\frac{\partial^2 c}{\partial y^2} + \frac{D_T}{T_\infty}\left(\frac{\partial^2 T}{\partial y^2}\right) - C_R\,[C - C_\infty] = 0$$

(4)

Boundary Conditions:

$$u = U(x), v = 0, T = T_W \text{ and } C = C_W \text{ at } y = 0$$

$$u \to 0, T \to T_\infty, C \to C_\infty \text{ as } y \to \infty \qquad (5)$$

Stream function of flow field

$$u = \frac{\partial \psi}{\partial y}, v = -\frac{\partial \psi}{\partial x} \qquad (6)$$

The following similarity transformations are employed to obtain dimensionless differential equations governing the flow model.

$$\eta = y\sqrt{\frac{a}{\nu}}, \psi = \sqrt{a\nu}\,x\,f(\eta), \theta = \frac{T - T_\infty}{T_W - T_\infty}, \Phi(\eta) = \frac{C - C_\infty}{C_W - C_\infty}$$

(7)

Using the variables in equations (6) and (7), the developed model is transformed into dimensionless equations as follows:

$$\alpha f''' - \alpha\beta f''^2 f''' - f'^2 + f f'' - (M+K)f' = 0$$
(8)

$$\theta'' + Pr\left(f\theta' + Nb\,\theta'\,\Phi' + Nt\,\theta'^2\right) = 0$$
(9)

$$\Phi'' + Le\,Prf\,\Phi' + \frac{Nt}{Nb}\theta'' - Kr\,\phi = 0$$
(10)

The dimensionless boundary conditions

$$f(0) = 0, f'(0) = 1, f'(\infty) = 0,$$
$$\theta(0) = 1, \theta(\infty) \to 0$$
$$\Phi(0) = 1, \Phi(\infty) \to 0 \qquad (11)$$

III. METHODOLOGICAL TECHNIQUE

A numerical shooting method is combined with the fourth-order Runge-Kutta technique to provide the overall solutions to the dimensionless boundary value derivative invariant coupled equations. This solution procedure has been employed following its suitability, stability, convergence, and precision in the unavailability of closed-form results, demonstrated by (Salawu [25]; Disu and Salawu [26]). The solution procedure involves the transformation of the boundary value model into an initial value derivative model by appropriately selection finite points $\eta \to \infty$ using shooting method. Afterwards, the Runge-Kutta scheme is introduced to solve the differential equations. A guess initial value is engaged with the unknown conditions equivalent to the $\phi(0), f(0)$ and $\theta(0)$. The computational process is repetitively done for diverse η_∞ values until the unknown successive values are determined. Hence, the differentials are redefined in first-order form as:

$$\gamma_1 = f, \gamma_2 = f', \gamma_3 = f'', \gamma_4 = \theta, \gamma_5 = \theta', \gamma_6 = \phi, \gamma_7 = \phi', \qquad (1)$$

$$\gamma_3' = \frac{\left(\gamma_2^2 - \gamma_1\gamma_3 + (M+K)\gamma_2\right)}{\alpha\left(1-\beta\gamma_3^2\right)}, \qquad (2)$$

$$\gamma_5' = -\Pr\left(\gamma_1\gamma_5 + Nb\gamma_5\gamma_7 + Nt\gamma_5^2\right), \qquad (3)$$

$$\gamma_7' = -LePr\gamma_1\gamma_7 - \frac{Nt}{Nb}\gamma_5' - Kr\gamma_6, \qquad (4)$$

The compatible boundary conditions give:

$$\gamma(0) = 0, \gamma_2(0) = 1, \gamma_4(0) = 1, \gamma_6(0) = 1, \gamma_2(\infty) \to 0, \gamma_4(\infty) \to 0, \gamma_6(\infty) \to 0. \qquad (5)$$

The boundary conditions are satisfied; a Maple symbolic code is developed to give a numerical solution for the flow model, following Salawu and Okoya [27]. The numerical convergence of the adopted solution scheme is given in Table 1. As noted in the table, a rapid solution converges at $\eta \to 4.0$ is obtained. Furthermore, to establish the exactness, consistency and precision of the solution methodology, a verification of the computed results with the allied numerical outputs is displayed in Table 2. The numerical values depict a robust agreement of the present and previous outcomes; thus, the results are given.

Table 1: Convergence iteration of the spectral weighted residual scheme

η	$f'(\eta)$	$\phi(\eta)$	$\theta(\eta)$
0.0	1.0000000000	1.0000000000	1.0000000000
0.1	0.0540957157	0.1056141879	0.3613711020
2.0	0.0029359432	0.0228579918	0.0469574525
3.0	0.0001568267	0.0024490185	0.0041354089
4.0	0	0	0
5.0	0	0	0

Table 2: Comparison of local wall shear rate against M while fixing fluid parameters α=1, β=0

M	Chamkha *et al.* [18]	Akbar *et al.* [14]	Rehman *et al.*	Present Results

			[15]	
0	-1.00000	-1.00000	-1.0040	-1.0000000
0.5	–	-1.11803	-1.1180	-1.1180287
1.0	-1.41412	-1.41421	-1.4140	-1.4142062
5.0	-2.44948	-2.44949	-2.4494	-2/4494878
10	-3.31662	-3.31663	-3.3168	-3.3166265

IV. RESULTS AND DISCUSSION

Figure 2 illustrates the influence of the magnetic parameter (M) on the dimensionless velocity profile. It is observed that increasing the magnetic field strength significantly suppresses the fluid velocity throughout the boundary layer. This behaviour is expected because the applied transverse magnetic field generates a Lorentz force that acts opposite to the direction of fluid motion. The resulting electromagnetic resistance increases momentum dissipation and reduces the kinetic energy of the fluid. Consequently, the momentum boundary layer becomes thinner, and the fluid approaches the ambient stationary condition more rapidly. This phenomenon is particularly useful in industrial processes requiring precise control of electrically conducting fluids, such as electromagnetic casting, cooling systems, and metallurgical operations. Figure 3 presents the variation of the velocity profile with the porous medium parameter (K). An increase in the porosity parameter reduces the fluid velocity within the boundary layer. Physically, the porous matrix introduces an additional drag force that opposes fluid motion according to Darcy's resistance law. The increased resistance diminishes fluid momentum and accelerates the decay of the velocity profile toward the free-stream condition. The results indicate that porous materials effectively regulate fluid transport, making them beneficial in filtration processes, geothermal reservoirs, catalytic reactors, and packed-bed heat exchangers where controlled fluid movement is desirable. Figure 4 depicts the effect of the Prandtl-Eyring fluid parameter (\alpha) on the velocity distribution. The results show that increasing (\alpha) enhances the velocity profile and enlarges the momentum boundary layer thickness. This behaviour is attributed to the non-Newtonian rheological characteristics of the Prandtl-Eyring fluid. Higher values of the material parameter reduce the effective resistance to deformation, thereby allowing the fluid to flow more freely under the stretching action of the surface. Consequently, momentum transport is enhanced, distinguishing the behaviour of Prandtl-Eyring fluids from that of conventional Newtonian fluids.

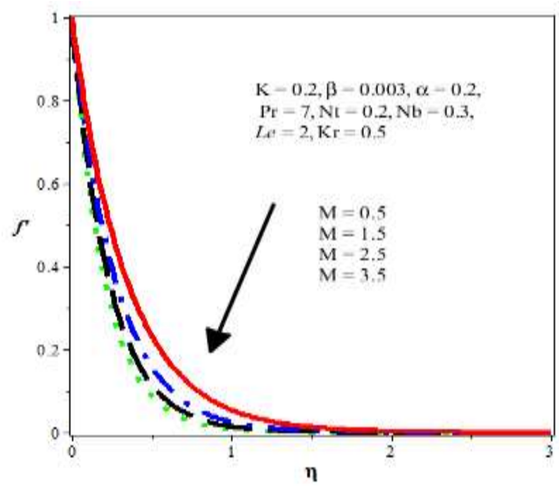

Figure 2: Impact of magnetic field (M) on the flow profile

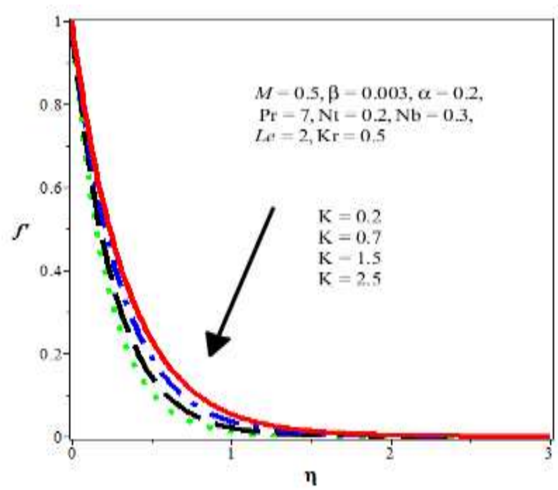

Figure 3: Effect porosity term (K) on the velocity field

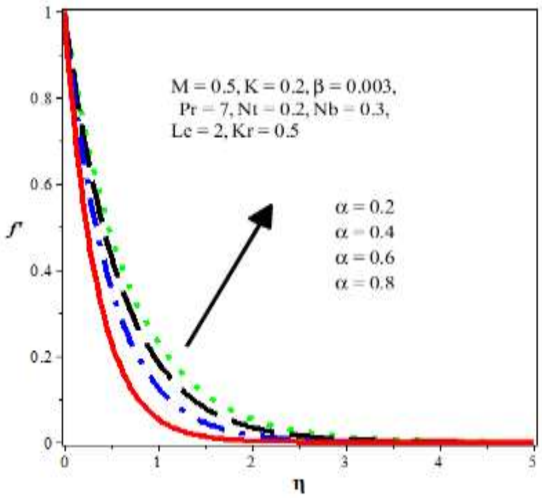

Figure 4: Prandtl-Eyring material term (α) on the flow distribution

Figure 5 demonstrates that increasing the Prandtl number decreases the temperature profile within the thermal boundary layer. The Prandtl number represents the ratio of momentum diffusivity to thermal diffusivity. Larger values of (Pr) correspond to lower thermal diffusivity, implying that heat diffuses less efficiently through the fluid. Consequently, thermal energy remains confined closer to the stretching surface, producing a thinner thermal boundary layer and lower fluid temperatures away from the wall. These findings indicate enhanced surface heat transfer for fluids with high Prandtl numbers, such as oils and polymeric liquids. Figure 6 shows that the temperature distribution increases significantly as the thermophoresis parameter (Nt) increases. Thermophoresis causes nanoparticles to migrate from hotter regions near the wall toward cooler regions in the surrounding fluid. This migration transports thermal energy into the fluid, thereby increasing the overall temperature and thickening the thermal boundary layer. The enhanced thermal diffusion observed confirms the dominant role of thermophoretic transport in nanofluid heat transfer and supports the improved thermal performance predicted by the Buongiorno nanofluid model. Figure 7 illustrates that increasing the Brownian motion parameter (Nb) elevates the fluid temperature throughout the thermal boundary layer. Brownian motion represents the random movement of nanoparticles suspended in the base fluid. As nanoparticle collisions become more intense, microscopic mixing is enhanced, promoting energy transport from the heated surface into the surrounding fluid. This increased thermal energy distribution results in a thicker thermal boundary layer and higher temperature profiles. The results demonstrate the significant contribution of Brownian diffusion to heat transfer enhancement in nanofluids.

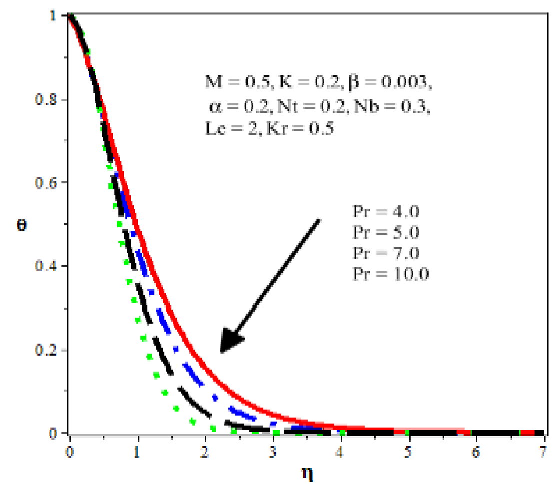

Figure 5: Prandtl number (Pr) effect on the heat transfer

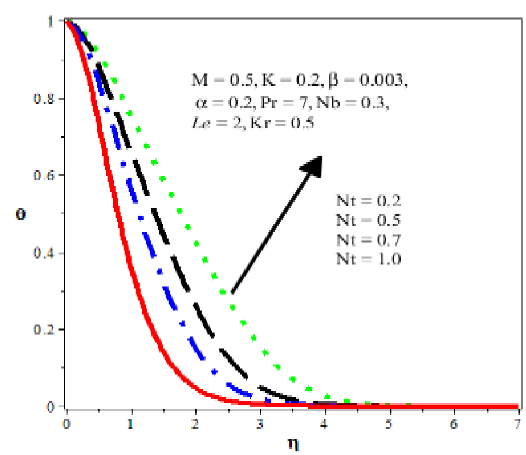

Figure 6: Influence of thermophoresis (Nt) on the temperature field

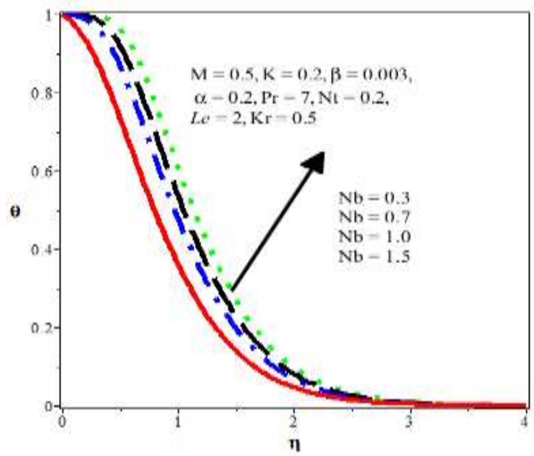

Figure 7: Brownian motion (Nb) impact on the thermal profile

Figure 8 presents the effect of thermophoresis on nanoparticle concentration. As the thermophoretic parameter increases, the concentration profile becomes larger and the concentration boundary layer thickens. Thermophoretic forces transport nanoparticles from the heated wall toward cooler fluid regions, thereby increasing nanoparticle accumulation within the boundary layer. This enhanced species transport delays concentration decay and extends the concentration boundary layer. Such behaviour is important in nanoparticle deposition, coating technologies, and targeted transport applications where particle migration plays a significant role. Figure 9 demonstrates that increasing the Lewis number reduces the nanoparticle concentration profile. The Lewis number is defined as the ratio of thermal diffusivity to mass diffusivity. Larger values of (Le) correspond to weaker mass diffusion, limiting nanoparticle transport within the fluid. Consequently, the concentration boundary layer becomes thinner, and the nanoparticle concentration decreases more rapidly with increasing distance from the stretching surface. This behaviour indicates reduced species diffusion in fluids possessing relatively low mass diffusivity. Figure 10 illustrates that stronger chemical reactions reduce the concentration profile considerably. As the chemical reaction parameter (Kr) increases, nanoparticles or reacting species are consumed at a faster rate, leading to a significant decrease in concentration throughout the boundary layer. The concentration boundary layer therefore becomes thinner due to enhanced species depletion. This result is consistent with first-order destructive chemical reactions commonly encountered in catalytic reactors, environmental remediation, pharmaceutical processing, and combustion systems, where reactant consumption dominates mass transport.

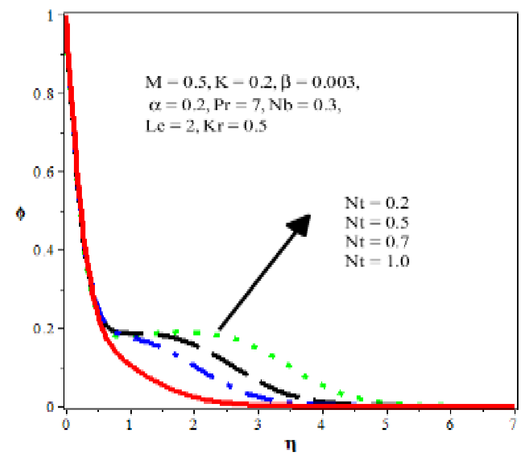

Figure 8: Impact of thermophoresis (Nt) on the mass transfer

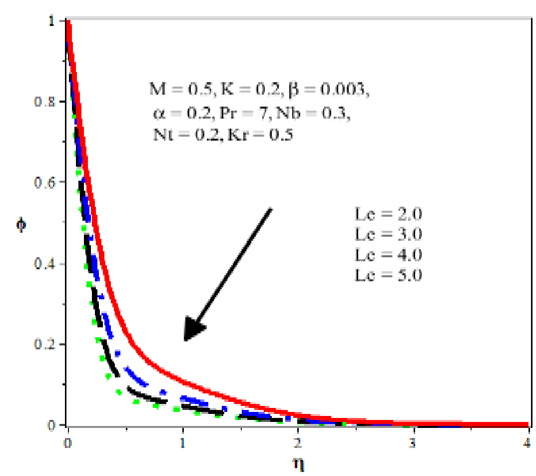

Figure 9: Effect Lewis number (Le) on the concentration profile

© JUL 2026 | IRE Journals | Volume 10 Issue 1 | ISSN: 2456-8880
DOI: https://doi.org/10.64388/IREV10I1-1719722

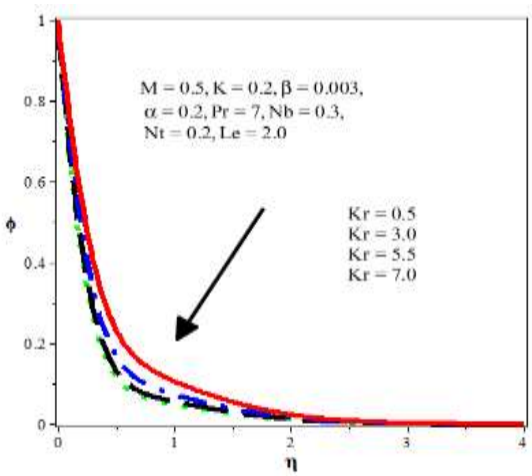

Figure 10: Chemical reaction term (Kr) effect on the species distribution

Figure 11 displays the streamline distribution describing the overall flow behaviour of the Prandtl-Eyring nanofluid over the stretching sheet. The streamlines remain smooth and continuous throughout the computational domain, confirming stable laminar flow without flow separation or recirculation. The dense clustering of streamlines near the stretching surface indicates strong velocity gradients and significant momentum transport within the boundary layer. Away from the wall, the streamlines gradually spread, illustrating the decay of momentum as the fluid approaches the ambient quiescent condition. The streamline pattern validates the physical consistency of the numerical solution. Figure 12 presents the temperature contour distribution within the flow domain. The thermal contours reveal that heat originates from the heated stretching sheet and diffuses progressively into the surrounding fluid. The closely spaced contours adjacent to the wall indicate steep temperature gradients and correspond to regions of high surface heat transfer. As the distance from the wall increases, the contours become more widely spaced, reflecting gradual thermal diffusion and reduced heat transfer intensity. The contour pattern clearly demonstrates the development of the thermal boundary layer and confirms the effectiveness of nanoparticle transport in enhancing heat propagation within the fluid. Figure 13 illustrates the two-dimensional concentration contours representing the mass transfer diffusion of nanoparticles in the Prandtl-Eyring nanofluid flowing over the stretching sheet. The contour lines describe the spatial distribution of nanoparticle concentration within the computational domain, while the colour gradient indicates the progressive reduction in concentration as the fluid moves away from the stretching surface. The concentration contours reveal that nanoparticle diffusion is strongest in the vicinity of the stretching sheet, where concentration gradients are highest. Near the wall, the contour lines are closely packed, indicating rapid mass transfer due to intense concentration gradients. As the fluid progresses downstream and farther from the wall, the contours become more widely spaced, demonstrating a gradual reduction in the concentration gradient and a corresponding decrease in the rate of nanoparticle diffusion. This behaviour is characteristic of boundary-layer mass transport, where molecular diffusion dominates near the surface but weakens as the species concentration approaches the ambient condition.

Table 3 demonstrates that the Prandtl-Eyring parameter and magnetic field strengthen surface shear stress, whereas the material parameter (\beta) slightly weakens it. These findings are important in engineering applications where minimizing drag or controlling wall shear is essential, including polymer extrusion, coating processes, electromagnetic cooling systems, and porous channel flows. Table 4 confirms that the Prandtl number enhances heat transfer, whereas Brownian motion and thermophoresis reduce the wall heat transfer rate by thickening the thermal boundary layer. These results are fully consistent with the temperature profiles presented in Figures 5-7 and demonstrate the competing influences of thermal diffusion and nanoparticle transport on heat transfer performance. The findings provide useful guidance for the design of nanofluid-based thermal systems, electronic cooling devices, heat exchangers, solar collectors, and chemically reactive transport processes where efficient thermal management is required.

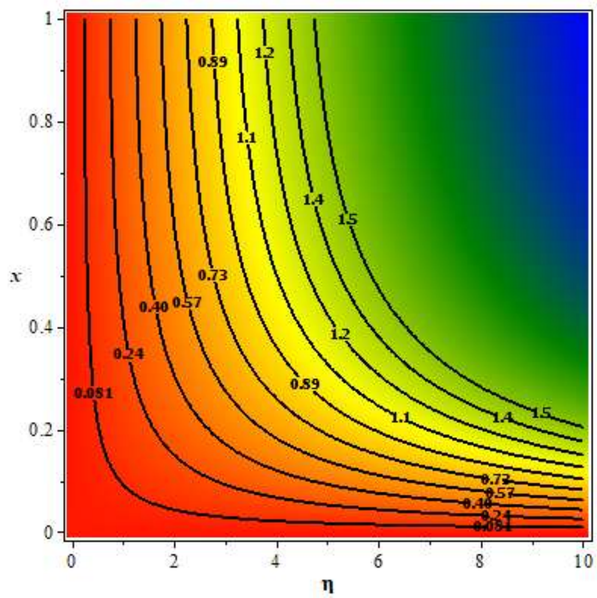

Figure 11: Streamlines flow pattern of the Prandtl-Eyring nanofluid

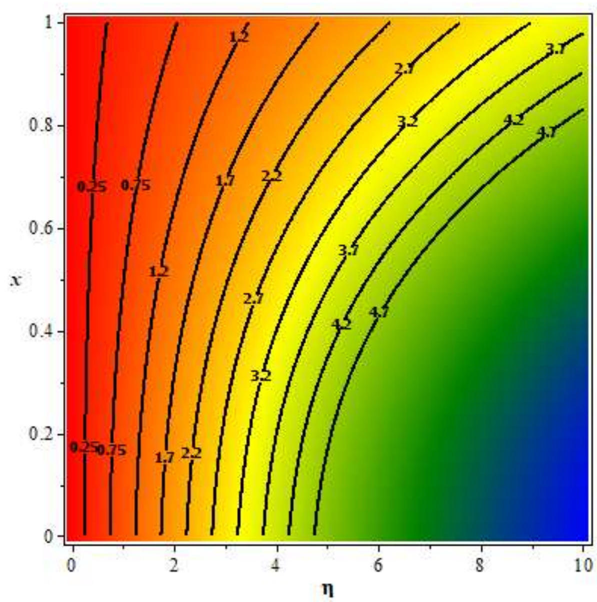

Figure 12: Heat propagation pattern of the Prandtl-Eyring nanofluid

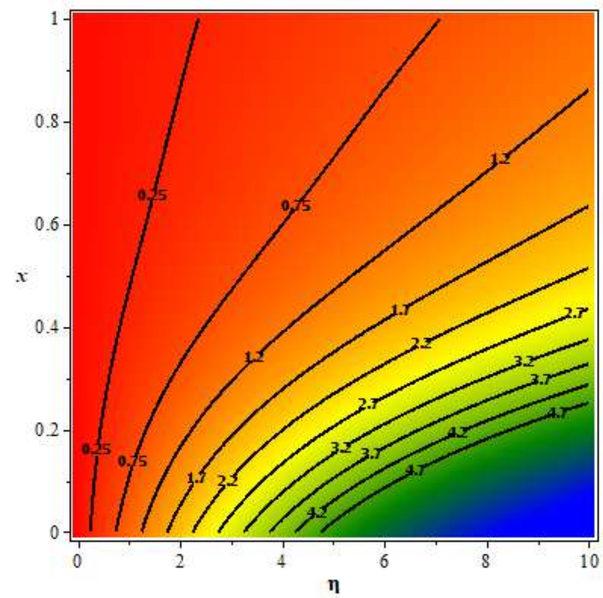

Figure 13: Mass transfer diffusion pattern for the Prandtl-Eyring nanofluid

Table 3: Coefficient of wall friction factor $|\alpha f''(0) - \frac{\alpha\beta}{3}(f''(0))^3|$ against variations in physical parameters α, β, and M

α	*β*	*M*	*Wall Friction Factor*
1.0	0.1	0.3	1.1259
1.5	0.1	0.3	1.3863
2.0	0.1	0.3	1.6067
3.0	0.1	0.3	1.9815
1.5	0.1	0.1	1.3863
1.5	0.2	0.1	1.3736
1.5	0.3	0.1	1.3597
1.5	0.4	0.1	1.3442
0.1	0.1	0.1	1.2785
0.1	0.3	0.1	1.3863

Table 4: Fluctuation in surface heat flux i.e. $-\theta' = 0$ by varying physical parameters Nb, Nt and Pr

Pr	*Nb*	*Nt*	*Surface Heat Flux* $-\theta' = 0$
2.0	0.1	0.1	0.7406
5.0	0.1	0.1	0.9060
7.0	0.1	0.1	1.1717
10.0	0.1	0.1	1.4522
2.0	0.1	0.2	0.6415
2.0	0.1	0.3	0.5538

2.0	0.1	0.5	0.4089
2.0	0.2	0.1	0.6840
2.0	0.3	0.1	0.6328
2.0	0.4	0.1	0.5866

V. CONCLUSION

This study investigated the steady two-dimensional magnetohydrodynamic (MHD) flow of a Prandtl-Eyring nanofluid over a stretching sheet embedded in a porous medium while incorporating Brownian motion, thermophoresis, and a first-order homogeneous chemical reaction based on the Buongiorno nanofluid model. The governing nonlinear partial differential equations were successfully transformed into a coupled system of ordinary differential equations using similarity transformations and solved numerically via the shooting method coupled with the classical fourth-order Runge-Kutta scheme. The numerical procedure was validated through comparison with previously published results, demonstrating excellent agreement and confirming the reliability and accuracy of the computational approach. The numerical results revealed that:

- The magnetic field and porous medium resistance significantly suppress fluid velocity due to the combined influence of the Lorentz force and Darcy resistance, leading to thinner momentum boundary layers and increased wall shear stress.
- Increasing the Prandtl-Eyring fluid term enhanced the velocity distribution, illustrating the influence of non-Newtonian rheology on momentum transport.
- Brownian motion and thermophoretic diffusion increased the thermal boundary-layer thickness through enhanced nanoparticle energy transport.
- The concentration field, increasing the Lewis number and the chemical reaction parameter reduced nanoparticle concentration by weakening mass diffusion and accelerating species consumption.
- Thermophoresis promoted nanoparticle migration and increased concentration within the boundary layer.

The findings contribute to the growing body of knowledge on non-Newtonian nanofluid dynamics and provide useful design guidelines for optimizing thermal management systems, porous heat exchangers, catalytic reactors, electronic cooling devices, polymer processing, energy conversion technologies, and other chemically reactive engineering applications involving electrically conducting non-Newtonian nanofluids. Future studies may extend the present model by incorporating variable thermophysical properties, nonlinear thermal radiation, viscous dissipation, Joule heating, activation energy, bioconvection, slip boundary conditions, unsteady flow, or hybrid nanofluids to further enhance its applicability to complex industrial and biomedical systems.

REFERENCES

[1] Choi, S.U.S. (1995). Enhancing thermal conductivity of fluids with nanoparticles. ASME FED 231, 99–105.

[2] Eastman, J.A., et al. (2001). Anomalously increased effective thermal conductivities of ethylene glycol-based nanofluids. Appl. Phys. Lett., 78(6), 718–720.

[3] Lee, S., et al. (1999). Measuring thermal conductivity of fluids containing oxide nanoparticles. J. Heat Transfer, 121(2), 280–289.

[4] Buongiorno, J. (2006). Convective transport in nanofluids. J. Heat Transfer, 128(3), 240–250.

[5] Khan, W.A., & Pop, I. (2010). Boundary-layer flow of a nanofluid past a stretching sheet. Int. J. Heat Mass Transf., 53(11-12), 2477–2483.

[6] Bachok, N., et al. (2010). Boundary layer flow of nanofluids over a moving surface. Int. J. Heat Mass Transf., 55(4), 807–813.

[7] Nadeem, S., et al. (2013). MHD flow of a nanofluid over a stretching sheet. Appl. Nanosci., 3, 213–220.

[8] Rashidi, M.M., et al. (2016). MHD nanofluid flow over a stretching sheet with chemical reaction. Ain Shams Eng. J., 7(1), 237–245.

[9] Wakif, A., et al. (2021). Thermal radiation and entropy generation in nanofluid flows. Case Stud. Therm. Eng., 25, 100891.

[10] Ellahi, R., et al. (2015). MHD flow of nanofluid with Joule heating. Appl. Math. Model., 39(1), 17–32.

[11] Mustafa, M., et al. (2012). Stagnation point flow of nanofluid with magnetic field. J. Thermophys. Heat Transf., 26(4), 691–697.

[12] Noghrehabadi, A., et al. (2013). Heat transfer in MHD nanofluid over a stretching surface. Heat Mass Transf., 49, 427–435.

[13] Hayat, T., et al. (2017). Prandtl-Eyring fluid flow over a nonlinear stretching surface. J. Mol. Liq., 225, 569–577.

[14] Akbar, N.S., et al. (2014). Prandtl-Eyringnanofluid over a stretching sheet. J. Comput. Theor. Nanosci., 11(2), 485–490.

[15] Rehman, K., et al. (2020). Influence of variable thermal conductivity on Prandtl-Eyringnanofluid. Results Phys., 16, 102869.

[16] Malik, M.Y., et al. (2015). Effects of magnetic field on Prandtl-Eyring fluid flow. J. Magn. Magn. Mater., 382, 355–360.

[17] Hayat, T., et al. (2018). Prandtl-Eyring fluid with mixed convection. Eur. Phys. J. Plus, 133, 388.

[18] Chamkha, A.J., et al. (2017). MHD nanofluid flow in porous media. Int. Commun. Heat Mass Transf., 86, 50–57.

[19] Raju, C.S.K., et al. (2018). Nanofluid flow over a porous stretching sheet. J. Braz. Soc. Mech. Sci. Eng., 40, 489.

[20] Das, K., (2011). Chemical reaction effects on nanofluid flow. Comput. Math. Appl., 62(2), 888–896.

[21] Ramzan, M., et al. (2017). MHD chemically reactive nanofluid flow with thermal radiation. J. Mol. Liq., 229, 161–168.

[22] Liao, S. (2003). Beyond perturbation: Introduction to the homotopy analysis method. CRC Press.

[23] Ganji, D.D., et al. (2014). Analytical techniques for nanofluid problems. Therm. Sci., 18(4), 1303–1310.

[24] Rashidi, M.M., et al. (2015). Approximate analytical solutions using the RKF method. J. Comput. Appl. Math., 276, 431–445.

[25] Salawu,S.O.(2023).Stagnation-point flow of Williamson fluid along a stretched plate with convective thermal condition and activation energy. Int. J. of Appl. Mech. and Engin. 28(3) 101-111.

[26] Disu, A.B., Salawu, S.O.(2023).Thermal distribution of magneto tangent hyperbolic flowing fluid over a porous moving sheet: Lie group analysis. J. of the Nig. Soc. of Phys. Sci., 5, 1103.

[27] Salawu S.O., Okoya, S.S. (2025): Exothermic diffusion-reaction and explosion branch-chain of an asymmetrical heating channel with convective cooling. Combut. Sci. and Techn. 197, 1154-1168.